water

MDPI

Article

Automatic Flood Monitoring Method with SAR and Optical Data Using Google Earth Engine

Xiaoran Peng [1], Shengbo Chen [1,*], Zhengwei Miao [2], Yucheng Xu [1], Mengying Ye [1] and Peng Lu [1]

[1] College of Geo-Exploration Science and Technology, Jilin University, Changchun 130026, China; pengxr22@mails.jlu.edu.cn (X.P.); ycxu21@mails.jlu.edu.cn (Y.X.); yemy22@mails.jlu.edu.cn (M.Y.); lupeng@jlu.edu.cn (P.L.)

[2] Key Laboratory of Digital Earth Science, Aerospace Information Research Institute, Chinese Academy of Sciences, Beijing 100094, China; miaozhengwei@home.hpu.edu.cn

* Correspondence: chensb@jlu.edu.cn

Abstract: Accurate and near-real-time flood monitoring is crucial for effective post-disaster relief efforts. Although extensive research has been conducted on flood classification, efficiently and automatically processing multi-source imagery to generate reliable flood inundation maps remains challenging. In this study, a new automatic flood monitoring method, utilizing optical and Synthetic Aperture Radar (SAR) imagery, was developed based on the Google Earth Engine (GEE) cloud platform. The Normalized Difference Flood Vegetation Index (NDFVI) was innovatively combined with the Edge Otsu segmentation method, utilizing SAR imagery, to enhance the initial accuracy of flood area mapping. To more effectively distinguish flood areas from non-seasonal water bodies, such as lakes, rivers, and reservoirs, pre-flood Landsat-8 imagery was analyzed. Non-seasonal water bodies were classified using multi-index methods and water body probability distributions, thereby further enhancing the accuracy of flood mapping. The method was applied to the catastrophic floods in Poyang Lake, Jiangxi Province, in 2020, and East Dongting Lake, Hunan Province, China, in 2024. The results demonstrated classification accuracies of 92.6% and 97.2% for flood inundation mapping during the Poyang Lake and East Dongting Lake events, respectively. This method offers efficient and precise information support to decision-makers and emergency responders, thereby fully demonstrating its substantial potential for practical applications.

Keywords: Sentinel-1; NDFVI; Edge Otsu; Landsat-8; non-seasonal water bodies; GEE

check for updates

Academic Editor: Xiaoping Rui

Received: 13 December 2024
Revised: 3 January 2025
Accepted: 8 January 2025
Published: 10 January 2025

Citation: Peng, X.; Chen, S.; Miao, Z.; Xu, Y.; Ye, M.; Lu, P. Automatic Flood Monitoring Method with SAR and Optical Data Using Google Earth Engine. *Water* **2025**, *17*, 177. https://doi.org/10.3390/w17020177

Copyright: © 2025 by the authors. Licensee MDPI, Basel, Switzerland. This article is an open access article distributed under the terms and conditions of the Creative Commons Attribution (CC BY) license (https://creativecommons.org/licenses/by/4.0/).

1. Introduction

Over the past two decades, approximately 4.2 billion people worldwide have been affected by natural disasters, resulting in economic losses of USD 2.97 trillion [1]. Among these, floods are considered among the most common and destructive natural disasters, representing a significant threat to ecosystem stability and the safety of human lives and property [2]. China, frequently affected by floods, was impacted by disasters caused by severe rainstorms and other factors in the first half of 2024, impacting 14.34 million people. Therefore, the research on advanced monitoring technologies is particularly urgent [3]. Accurate and efficient flood monitoring, as well as the acquisition of information on affected areas, is crucial for post-disaster rescue and evaluation [4,5].

Traditional flood emergency monitoring methods are often constrained by the complex environments of affected areas, thereby complicating rapid implementation [6]. With the ongoing advancement of satellite-based remote sensing technology, the application of

multi-source satellite remote sensing data in flood monitoring has become increasingly prevalent. These technologies enable effective and accurate monitoring of flood events, thus supporting rapid response efforts [7,8]. Flood monitoring is primarily conducted using optical imagery that utilizes spectral information to analyze differences between water and non-water bodies, facilitating flood mapping. Water indices commonly used include the Normalized Difference Water Index (NDWI) [9], the Modified Normalized Difference Water Index (MNDWI) [10], and the Enhanced Water Index (EWI) [11], among others. However, due to geographical and time-related variations, the spectral characteristics of water bodies in optical imagery are subject to continuous change, making it relatively challenging to distinguish water bodies from non-water bodies using a single threshold [12]. Additionally, multiple vegetation and water indices are integrated in some studies, such as the Enhanced Vegetation Index (EVI), the Normalized Difference Vegetation Index (NDVI), the Modified Normalized Difference Water Index (MNDWI), and the Automated Water Extraction Index (AWEI) to classify water bodies [13,14]. These methods are typically utilized to extract long-term changes in surface water and have demonstrated favorable results. However, during flood events, the frequent occurrence of cloudy or rainy weather restricts the observational capabilities of optical remote sensing satellites, complicating the delineation of flooded areas using these methods [15,16].

Unlike optical imagery, which is frequently obscured by clouds and rain, Synthetic Aperture Radar (SAR) data are unaffected by adverse weather conditions. Due to this advantage, they have garnered extensive attention in disaster monitoring [17–19]. Several methods have been proposed for flood mapping using SAR data, including backscatter threshold algorithms, supervised classification [20], fuzzy logic classification [21], and region growing [22]. Most techniques rely on single-temporal imagery for flood detection; however, multi-temporal approaches that combine pre- and post-flood SAR data can produce more accurate flood maps [23–25]. Therefore, SAR change detection is a widely used image analysis method for identifying changes in water bodies by comparing imagery from different dates [26]. Techniques such as the Normalized Difference Flood Vegetation Index (NDFVI), the Normalized Difference Flood Index (NDFI), the Ratio Image (RI), and the Difference Image Index (DII) have been utilized in studies [27,28]. Imagery from different dates is leveraged by these methods to identify changes in water areas, effectively detecting regions affected by flooding [29]. SAR change detection methods typically consist of two main components. Initially, a change detection image is generated. Subsequently, supervised or unsupervised classification techniques are employed to classify the change detection image [30]. Although supervised classification methods provide high accuracy, they require manual extraction of training samples and have limited applicability across different regions [31]. In contrast, unsupervised classification methods offer greater generalizability, which makes them more suitable for rapid flood monitoring [32]. Classifying flood areas using SAR data presents several challenges. Wind and heavy rainfall can temporarily shape a roughness on the water surface and hinder flood delineation [33]. Additionally, strong backscatter signals in vegetated or densely urban areas cause these regions to appear unusually bright, complicating classification. Furthermore, similar backscatter coefficient values among various features lead to inaccuracies in delineating water body boundaries. Consequently, reliance on a single remote sensing data source increases the risk of misclassification [34].

Significantly enhancing the accuracy of flood monitoring are the complementary characteristics of optical and SAR imagery [35]. Studies have indicated that combining pre-flood optical images with radar images during the flood effectively compensates for the absence of optical imagery during flooding [36]. By employing change detection using radar imagery during floods, alongside pre-flood optical images, classification accuracy is

improved. Although change detection methods can provide clear images of flooded areas, the selection of thresholds must be adjusted according to the affected region, presenting certain limitations. Thus, adaptive threshold methods are more advantageous for rapid flood monitoring [37]. The Otsu threshold method was compared with machine learning approaches by Bangira et al., demonstrating the capability of automatic Otsu thresholding for water body detection using Sentinel-1 SAR data [38]. Despite the application of the Otsu threshold classification method to both optical and radar images for flood classification, improvements in classification results are still necessary [39]. Moreover, obtaining high-quality optical images during floods remains challenging, with significant variability in image availability across different regions. Some studies have applied the Edge Otsu method for surface water classification, showing better performance compared to Otsu and Bmax Otsu classification methods [39,40]. However, the Edge Otsu method has not yet been applied to flood monitoring using multi-source remote sensing data. Therefore, it is crucial to select an easily operable automated classification method that integrates multi-source remote sensing data.

This study proposes a scalable, replicable, and user-friendly method that utilizes the Google Earth Engine platform. The method innovatively combines NDFVI change detection with the Edge Otsu method by employing Sentinel-1 data to classify flood areas. To better distinguish flood zones from non-seasonal water bodies, pre-flood Landsat-8 imagery was utilized to integrate multi-index and probability distribution methods for the classification of non-seasonal water bodies, thereby further optimizing the flood classification results obtained from Sentinel-1. This study was applied to major flood events in the East Dongting Lake area of Hunan Province and the Poyang Lake area of Jiangxi Province, thereby aiding decision-makers and emergency planners in rapidly assessing the impacts of extreme flood events.

2. Materials and Methods

2.1. Study Areas

Dongting Lake and Poyang Lake are significant freshwater lakes situated in the middle section of the Yangtze River. They are recognized internationally as important wet-lands and habitats for rare migratory birds [41]. These lakes play crucial roles in climate regulation, water conservation, environmental purification, maintaining biodiversity within the Yangtze River basin, and supporting high-quality regional economic and social development (Figure 1) [42]. Poyang Lake, situated in Jiangxi Province, is the largest freshwater lake in China. In July 2020, continuous heavy rainfall resulted in significantly elevated water levels, which led to extreme flooding. Dongting Lake, situated in Hunan Province, ranks as the second-largest freshwater lake in China. On 5 July 2024, Dongting Lake experienced its first significant flood of the year. In recent years, floods have posed significant threats to human life and have caused substantial property damage. By utilizing the flood events in East Dongting Lake and Poyang Lake as case studies, the analysis of flood inundation areas is deemed crucial for the promotion of national sustainable development.

2.2. Data

2.2.1. Sentinel-1 SAR Data

Sentinel-1 SAR data are freely available and offers high resolution, providing Level-1 Ground Range Detected (GRD) products. These GRD products are extensively utilized for analyzing land cover backscatter and monitoring water bodies [24,43]. In this study, Sentinel-1 SAR data from before and after the floods were obtained using Google Earth Engine ("COPERNICUS/S1_GRD") (Table 1). The VH polarization of Sentinel-1 SAR data is commonly employed for reliable flood mapping, as it enhances contrast between water

bodies and surrounding features, such as vegetation and bare ground, thus facilitating differentiation. Data with VH polarization and the Interferometric Wide (IW) swath acquisition mode were utilized. To mitigate granular noise, the Lee-Sigma speckle filter was applied during preprocessing, and terrain correction was performed to remove topographic shadows before flood extent classification [39].

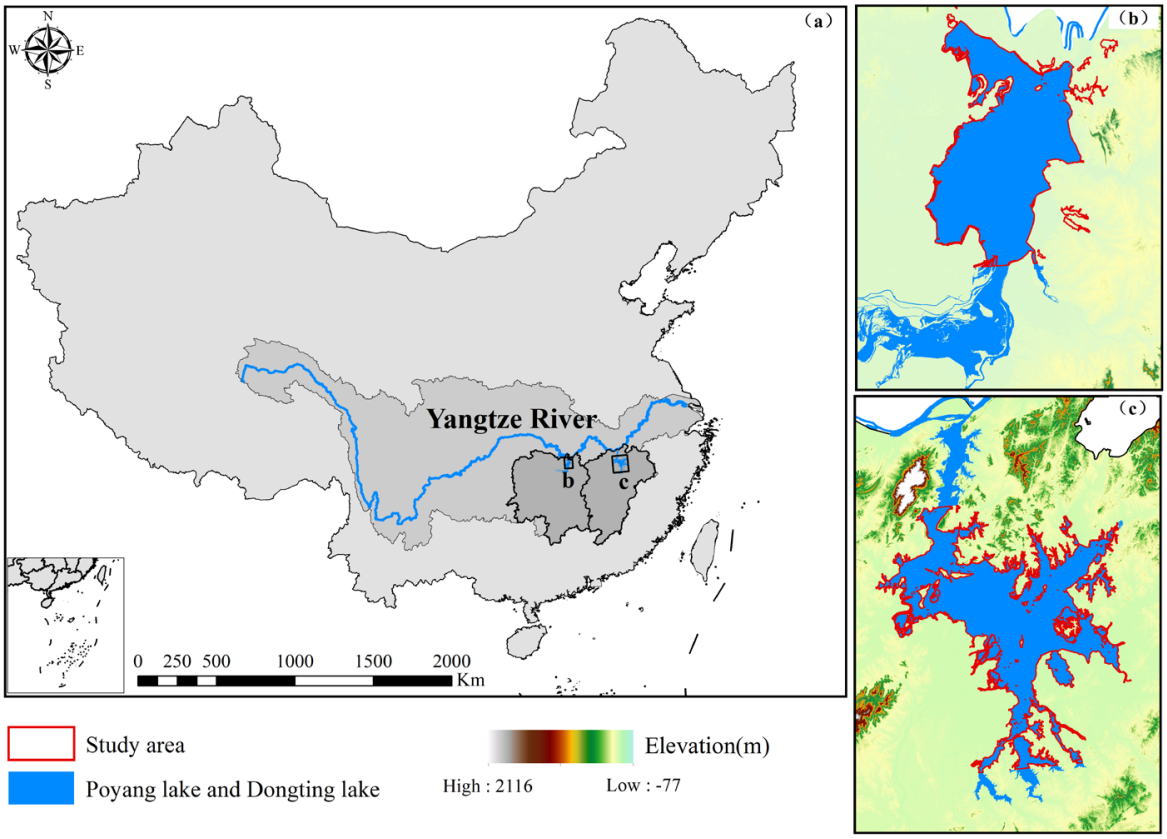


Figure 1. The geographical location of the study areas in China. (**a**) Location of the study area in China, (**b**) Extent of the Dongting Lake study area, (**c**) Extent of the Poyang Lake study area.

Table 1. List of images employed in flood monitoring.

Sensor	Date and Region	Status	Spatial Resolution
Sentinel-1	1 May 2020, Poyang River	Before flood	10 m
	15 June 2020, Poyang River		
	1 July 2020, Poyang River	After flood	
	10 July 2020, Poyang River		
	1 January 2024, East Dongting river	Before flood	10 m
	1 June 2024, East Dongting river		
	1 July 2024, East Dongting river	After flood	
	10 July 2024, East Dongting river		
Landsat-8	30 January 2017, Poyang River	Before flood	30 m
	30 January 2020, Poyang River		
	30 June 2021, East Dongting river	After flood	30 m
	30 May 2024, East Dongting river		

2.2.2. Landsat-8 Data

In this study, the Landsat-8 dataset was used to provide orthorectified surface reflectance images with a resolution of 30 m. The Operational Land Imager (OLI) includes 9 bands, which support the calculation of various remote sensing indices [44,45]. The Landsat-8 dataset ("Landsat/LC08/C01/T1_SR") provided by the USGS and accessible via the Google Earth Engine (GEE) platform was employed to acquire images of Poyang Lake from 2017 to 2020 and East Dongting Lake from 2021 to 2024 (Table 1), for classifying non-seasonal water bodies in the study areas.

2.2.3. Validation Data

The Sentinel-2 satellite is extensively utilized in flood monitoring and emergency response. By employing false-color composites of visible and near-infrared bands, water bodies can be clearly identified in vegetated areas, simplifying the visual interpretation process and enabling the generation of high-quality sampling points [46,47]. The Global Surface Water Dataset (GSWD) provides precise information on global surface water (available online: https://global-surface-water.appspot.com, accessed on 1 October 2024) [48]. The dataset's long-term product, with a 30 m resolution, is employed to illustrate the global spatiotemporal dynamics of lakes from 1984 to 2020. The global water surface dataset is an essential resource for monitoring and analyzing surface water dynamics and is suitable for validating water body classification results. In this study, the selection of validation points for the Poyang Lake region was based on the combination of the Sentinel-2 dataset on the Google Earth Engine platform and the Global Surface Water dataset. For the East Dongting Lake region, the validation points were selected using the Sentinel-2 dataset.

2.3. Methods

The workflow of the method proposed in this study is depicted in Figure 2 and is composed of four primary stages: preprocessing, flood classification using Sentinel-1 data, non-seasonal water body classification using Landsat-8 data, and accuracy validation.

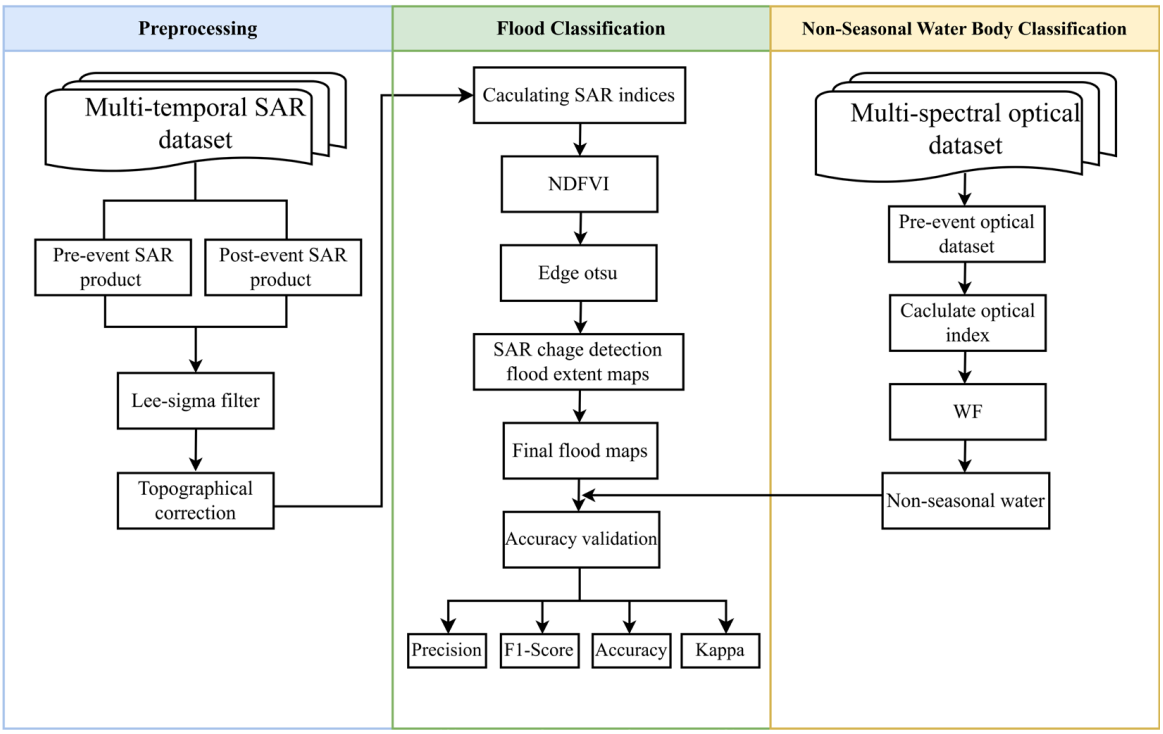


Figure 2. Flow diagram illustrating the overall approach employed in this study.

2.3.1. Preprocessing

A Lee-sigma filter was applied to the images to suppress speckle noise, effectively balancing the retention of spatial details and the enhancement of the signal-to-noise ratio [39]. Two mature physical reference models were adopted on the GEE platform to implement radiation tilt correction based on Sentinel-1 satellite data [49]. The models systematically describe the angular relationship between SAR images and terrain geometric features. The implementation of the models first requires the calculation of four key angular parameters, which enable an accurate description and correction of the geometric relationship between the SAR images and the terrain.

2.3.2. Automated Flood Inundation Classification with NDFVI and the Edge Otsu Method

The preprocessing of Sentinel-1 data involved radiometric correction, filtering, and terrain correction, followed by the calculation of the NDFVI index [27]. The NDFVI is a change detection method that compares backscatter intensity before and after a flood to detect pixel-level variations, which is effectively employed to precisely delineate flood inundation areas [27,50]. First, the average backscatter signal for each pixel in the pre-flood Sentinel-1 imagery is calculated. Subsequently, the maximum backscatter signal of each pixel in the post-flood Sentinel-1 imagery is computed to generate the post-flood NDFVI imagery. This method effectively captures changes in reflectance before and after the flood, facilitating the accurate delineation of flood-affected areas. The formula for calculation is as follows:

$$\mathrm{NDFVI} = \frac{|\max(\mathrm{afterflood})| - |\mathrm{mean}(\mathrm{beforeflood})|}{|\max(\mathrm{afterflood})| + |\mathrm{mean}(\mathrm{beforeflood})|} \quad (1)$$

In this context, max(afterflood) denotes the maximum backscatter value in the post-flood image, while mean(beforeflood) represents the average backscatter value in the pre-flood image.

To achieve automated and accurate flood inundation classification, NDFVI was combined with the Edge Otsu method. The Edge Otsu method, as introduced by Donchyts et al. [51], combines the Canny edge detection algorithm with Otsu's thresholding technique. Edge Otsu has been shown to perform better than the standard or other optimized Otsu methods under similar conditions [40]. It is widely utilized for generating high-quality surface water distribution maps, demonstrating reliable results [39]. In this study, the application of the Edge Otsu method was innovatively extended to NDFVI imagery for generating high-resolution flood inundation maps. Initially, the NDFVI imagery undergoes binarization for preprocessing. Subsequently, the Canny edge detection algorithm is applied to accurately delineate the contours and boundaries of the flood-affected areas. Following edge detection, a buffer analysis is conducted to efficiently collect sampling points for histogram construction. Finally, the Otsu method is employed to analyze the histogram of the buffered edge region, thereby determining the optimal threshold across the entire NDFVI imagery, which enables the automated classification of flood areas.

2.3.3. Optimization of Flood Inundation Classification Using Landsat-8 Data

Although the combination of NDFVI and the Edge Otsu method effectively delineates flood boundaries, it exhibits a tendency to overclassify non-seasonal water bodies, including rivers and lakes, within flooded regions. To mitigate this issue, Landsat-8 imagery was employed to integrate multi-index methods with the probability distribution for extracting non-seasonal water bodies, thus masking erroneously classified regions. The study by Yue et al. referenced NDWI, AWEI, NDVI, and EVI to develop a multi-index surface water classification standard [52]. The multi-index surface water classification criteria are defined as follows: ($\mathrm{AWEI_{nsh}}$—$\mathrm{AWEI_{sh}} > -0.1$) and (MNDWI > NDVI or MNDWI > EVI). This

rule was applied to the pre-flood Landsat-8 imagery for surface water classification. If the computed results met the specified criteria, the pixels were classified as water. Otherwise, they were classified as non-water. The definitions of these indices are as follows:

$$\mathrm{AWEI_{nsh}} = 4 \times (\rho_{\mathrm{GREEN}} - \rho_{\mathrm{SWIR1}}) - (0.25 \times \rho_{\mathrm{NIR}} - 2.75 \times \rho_{\mathrm{SWIR2}}) \quad (2)$$

$$\mathrm{AWEI_{sh}} = \rho_{\mathrm{BLUE}} + 2.5 \times \rho_{\mathrm{GREEN}} - 1.5(\rho_{\mathrm{NIR}} + \rho_{\mathrm{SWIR1}}) - 0.25 \times \rho_{\mathrm{SWIR2}} \quad (3)$$

$$\mathrm{NDVI} = \frac{\rho_{\mathrm{NIR}} - \rho_{\mathrm{RED}}}{\rho_{\mathrm{NIR}} + \rho_{\mathrm{RED}}} \quad (4)$$

$$\mathrm{MNDWI} = \frac{\rho_{\mathrm{GREEN}} - \rho_{\mathrm{SWIR}}}{\rho_{\mathrm{GREEN}} + \rho_{\mathrm{SWIR}}} \quad (5)$$

$$\mathrm{EVI} = 2.5 \times \frac{\rho_{\mathrm{NIR}} - \rho_{\mathrm{RED}}}{\rho_{\mathrm{NIR}} + 6 \times \rho_{\mathrm{RED}} - 7.5\rho_{\mathrm{BLUE}} + 1} \quad (6)$$

Among them, ρRED, ρGREEN, ρBLUE, ρNIR, ρSWIR1, and ρSWIR2 represent the reflectance of the red band, green band, blue band, near-infrared band, the short-wave infrared band 1, and the short-wave infrared band 2, respectively.

Landsat-8 imagery was analyzed to identify surface water bodies in two regions: the Poyang Lake area (30 January 2017 to 30 January 2020) and the East Dongting Lake area (30 June 2021 to 30 May 2024). Remote sensing indices were computed to delineate sur-face water distributions for these periods. The probability distribution of surface water was derived based on these indices. Pixels exhibiting a water probability exceeding 0.75 were classified as non-seasonal water bodies [53]. The probability density distribution function employed in this study is defined as follows:

$$\mathrm{WF} = \frac{\mathrm{N_{m(t_a,t_b)}}}{\mathrm{N_{n(t_a,t_b)}}} \quad (7)$$

Here, $\mathrm{N_{m(ta,tb)}}$ denotes the occurrences of each pixel in the study area meeting the surface water condition across all images, while $\mathrm{N_{n(ta,tb)}}$ refers to the total image count in the study area. Here, ta represents the start date and tb indicates the end date.

The extracted non-seasonal water bodies served as a mask to refine the initial flood classification results derived from the Edge Otsu method. This masking step effectively mitigates errors arising from overclassification, thereby enhancing the accuracy of flood delineation. The novel method proposed in this study, based on the GEE platform, effectively incorporates non-seasonal water bodies as an exclusion layer, while maintaining the good effect of the Edge Otsu method in identifying flood-affected areas within NDFVI imagery.

2.3.4. Accuracy Evaluation

Sentinel-2 imagery with 10 m spatial resolution was utilized on the GEE platform, in conjunction with the visual interpretation of water and non-water sample points, to assess the classification accuracy. The Global Surface Water dataset, updated until 2020, was used to assist in selecting sample points for Poyang Lake flood events. Confusion matrix-based evaluation parameters, including precision, accuracy, F1-score, and Kappa coefficient, were considered to evaluate the performance of the novel method [54]. These metrics collectively form a comprehensive evaluation framework to assess model performance from multiple dimensions [55,56].

$$\mathrm{Accuracy} = \frac{\mathrm{TP} + \mathrm{TN}}{\mathrm{TP} + \mathrm{TN} + \mathrm{FP} + \mathrm{FN}} \quad (8)$$

$$\mathrm{F1-score} = \frac{2 \times \mathrm{Precision} \times \mathrm{Recall}}{\mathrm{Precision} + \mathrm{Recall}} \quad (9)$$

$$\text{Precision} = \frac{\text{TP}}{\text{TP} + \text{FP}} \tag{10}$$

$$\text{Recall} = \frac{\text{TP}}{\text{TP} + \text{FN}} \tag{11}$$

$$\text{Kappa} = \frac{\text{p}_0 - \text{p}_\text{e}}{1 - \text{p}_\text{e}} \tag{12}$$

$$\text{p}_o = \frac{\text{TP} + \text{TN}}{\text{N}} \tag{13}$$

$$\text{p}_\text{e} = \frac{[(\text{TP} + \text{FP})(\text{TP} + \text{FN}) + (\text{TN} + \text{FP})(\text{TN} + \text{FN})]}{\text{N}^2} \tag{14}$$

TP, TN, FP, and FN denote the true positive, true negative, false positive, and false negative, respectively, and N is the total number of pixels in the image. p_o is the proportion of correctly classified pixels and p_e is the expected probability of agreement when the classifier labels classes at random.

3. Results

3.1. Flood Inundation Map Using Sentinel-1 SAR Data

Preprocessed Sentinel-1A SAR images were utilized to derive the pre-flood mean and post-flood maximum values. Figure 3a presents the mean of images before the 2020 Poyang Lake flood (from 1 May to 15 June 2020). Figure 3b shows the maximum of images after the 2020 Poyang Lake flood (from 1 to 10 July 2020). Figure 3c displays the mean of images before the 2024 East Dongting Lake flood (from 1 January to 1 June 2024), and Figure 3d shows the maximum of images after the 2024 East Dongting Lake flood (from 1 to 10 July 2024).

The NDFVI is calculated using Equation (1). Figure 4a illustrates the 2020 Poyang Lake NDFVI image, and Figure 4b illustrates the 2024 East Dongting Lake NDFVI image. The newly formed black patches (representing flooded areas), resulting from low backscatter signals, are clearly visible when comparing Figure 4a,b.

Flooded pixels in the SAR index images were mapped by initial classifying of the water and non-water areas in the NDFVI images of Poyang Lake and East Dongting Lake using the Edge Otsu method, resulting in the flood inundation classification map. Figure 5a illustrates the classification results for Poyang Lake, whereas Figure 6a depicts the classification results for East Dongting Lake. The blue areas represent the flooded regions.

During extended periods of heavy rainfall, the water levels of the lake increase rapidly, river channels expand, and large areas of villages become submerged. The East Dongting Lake flood predominantly affects the southern region, while the Poyang Lake flood is primarily concentrated on the eastern side. The classification results of this study demonstrate a high degree of spatial consistency with the actual affected areas, suggesting that the application of NDFVI and the Edge Otsu method for flood classification leads to effective outcomes.

Although the combined application of NDFVI and Edge Otsu in flood classification offers certain advantages, some limitations still remain. As shown in Figures 5b,c and 6b,c, a comparison of the local flood classification map with the pre-flood Sentinel-1 image of the area reveals that some non-seasonal water bodies, such as meandering and small rivers and lakes, are misclassified as flooded regions, as shown in the red-boxed areas in Figures 5 and 6.

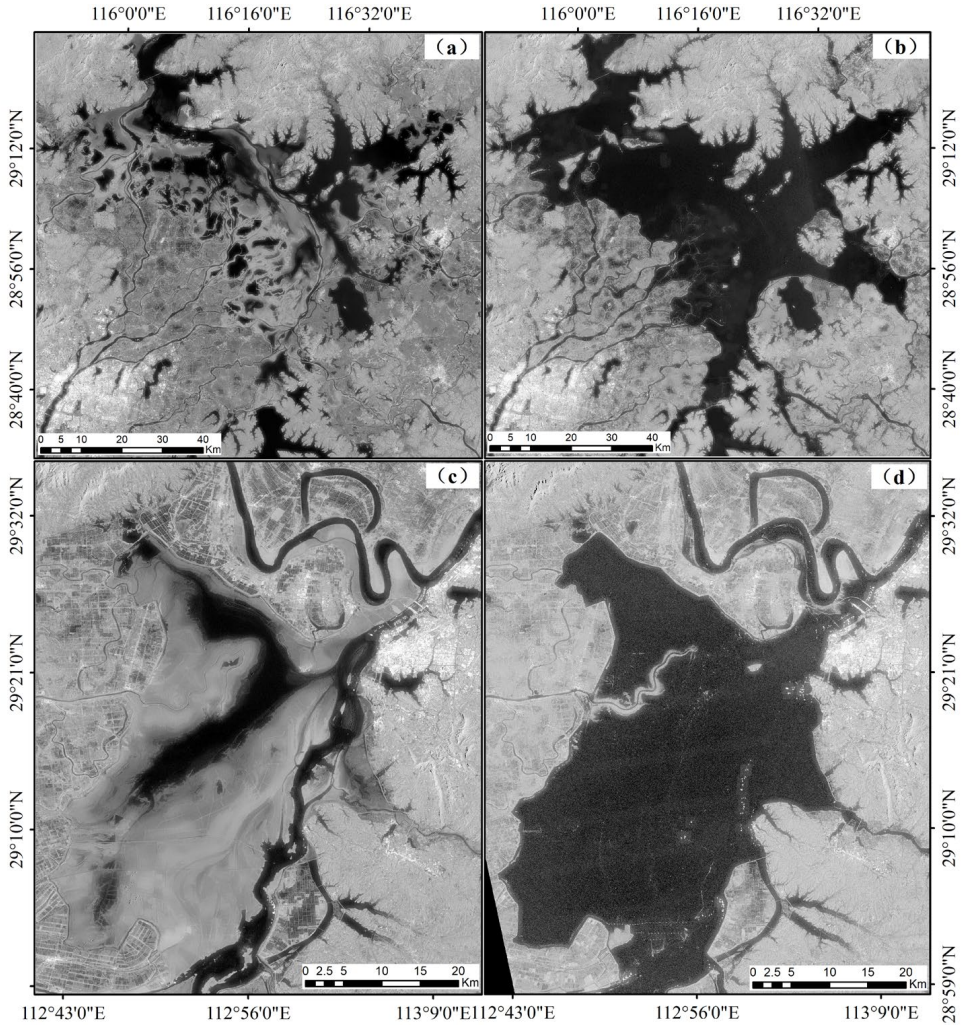


Figure 3. SAR images captured before and after the flood across multiple time periods. (**a**) The pre-flood average image of Poyang Lake, (**b**) The post-flood maximum value image of Poyang Lake, (**c**) The pre-flood average image of East Dongting Lake, (**d**) The post-flood maximum value image of East Dongting Lake.

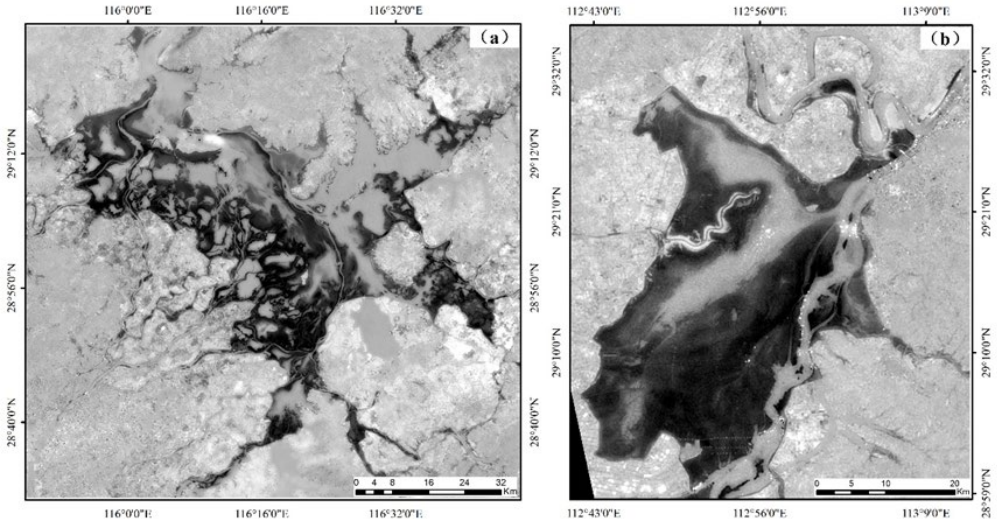


Figure 4. Results of NDFVI method. (**a**) The NDFVI image of Poyang Lake, (**b**) The NDFVI image of East Dongting Lake.

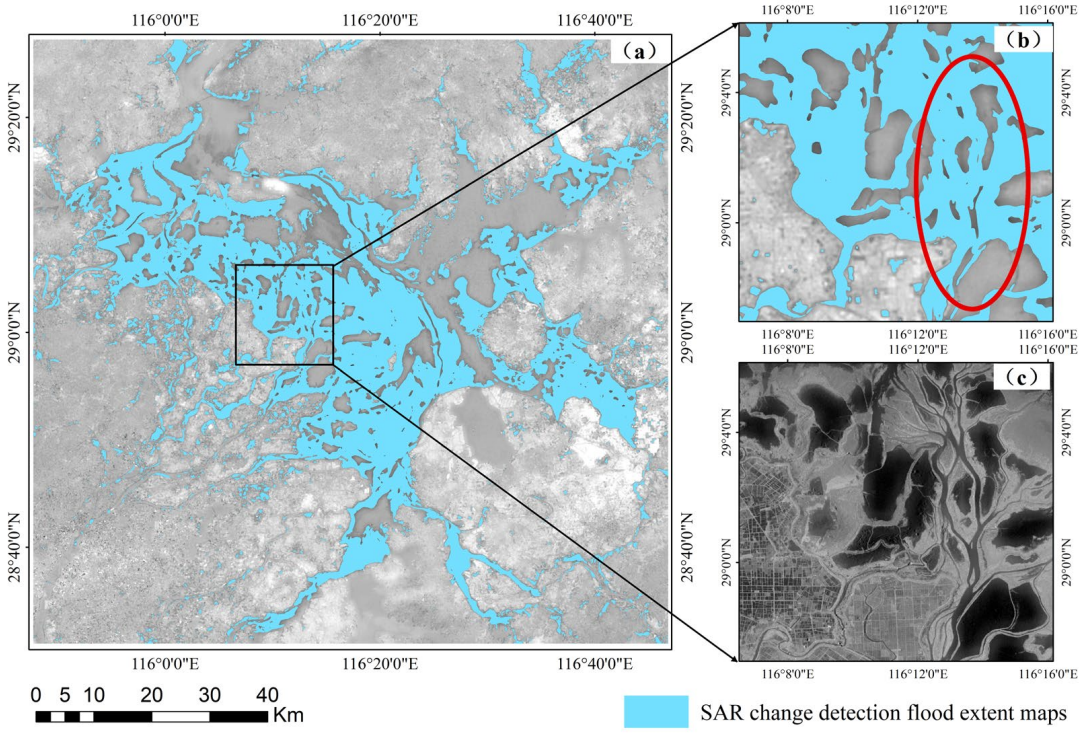


Figure 5. Flood classification results for Poyang Lake using Sentinel-1 image in 2020. (**a**) Flood classification results for Poyang Lake, (**b**) Local flood classification results for Poyang Lake, (**c**) Local Sentinel-1 imagery of Poyang Lake before the flood.

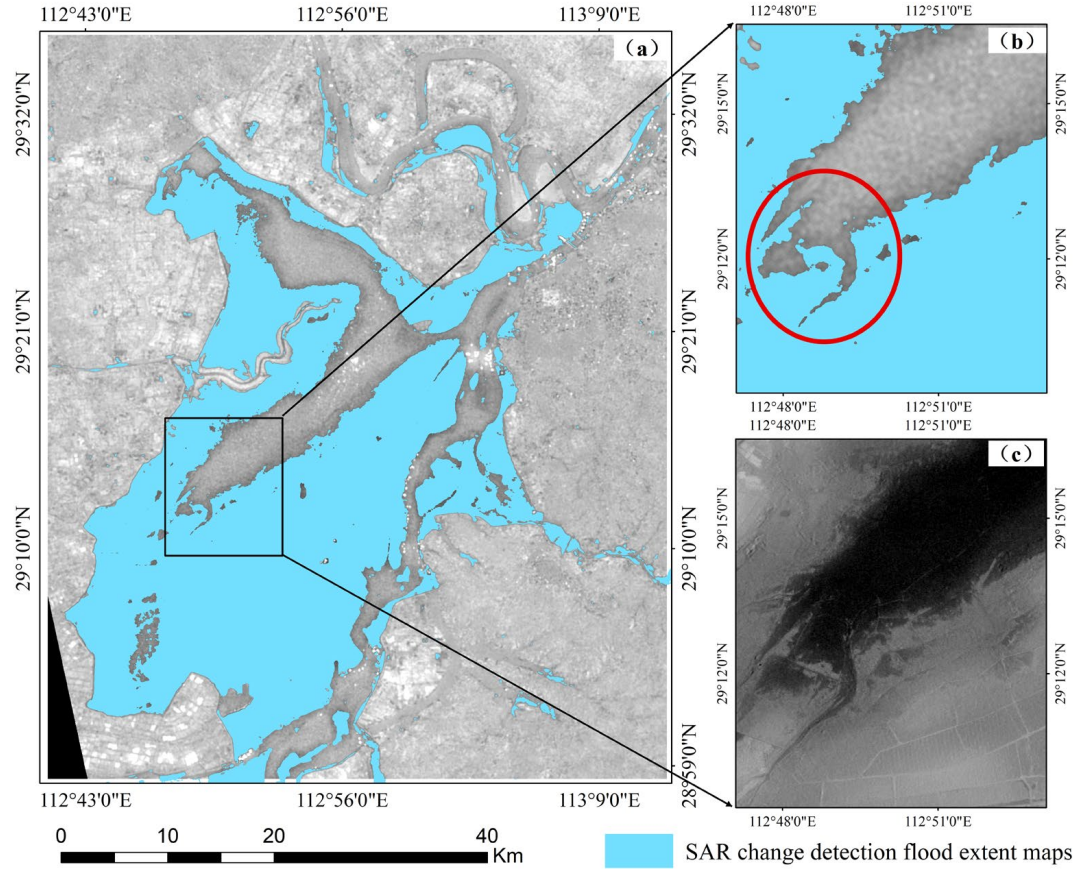


Figure 6. Flood classification results for East Dongting Lake using Sentinel-1 image in 2024. (**a**) Flood classification results for East Dongting Lake, (**b**) Local flood classification results for East Dongting Lake, (**c**) Local Sentinel-1 imagery of East Dongting Lake before the flood.

3.2. Optimizing Flood Classification Results Using Landsat-8 Data

After clouds are removed from the Landsat-8 images, areas meeting the multi-index criteria are classified as water bodies. Subsequently, all water body distribution maps are overlaid to calculate the probability of water bodies. When the probability exceeds 0.75 [53], the pixel is classified as a non-seasonal water body. The final non-seasonal water body area of Poyang Lake in the study area is 2337.58 square kilometers, while the non-seasonal water body area of East Dongting Lake in the study area is 1233.69 square kilometers. Figure 7a shows the spread of non-seasonal water in the Poyang Lake region, while Figure 7b shows the spread in the East Dongting Lake region.

Then, the final flood inundation area distribution maps were derived by masking the flood inundation area maps of Poyang Lake and East Dongting Lake with the non-seasonal water body maps. Figure 8 shows the results of the final flood classification map. The blue areas are indicative of the regions affected by flooding.

3.3. Precision Evaluation

Three traditional methods for flood extent classification using change detection were selected for comparative analysis: NDFI, RI, and DII. These methods were combined with threshold classification techniques to delineate flood inundation areas [36]. The comparison of this study's method with NDFI, RI, and DII is shown in Figure 9. The black areas in Figure 9 are classified as flood inundation areas. The "Our Results" column in Figure 9 displays the final flood inundation map, which was obtained using the method proposed in this study. Compared to the method in this study, the final flood classification maps derived using NDFI, RI, and DII methods exhibit boundary omissions and misclassification of some permanent water bodies as flood inundation areas. These errors have been effectively eliminated in this study.

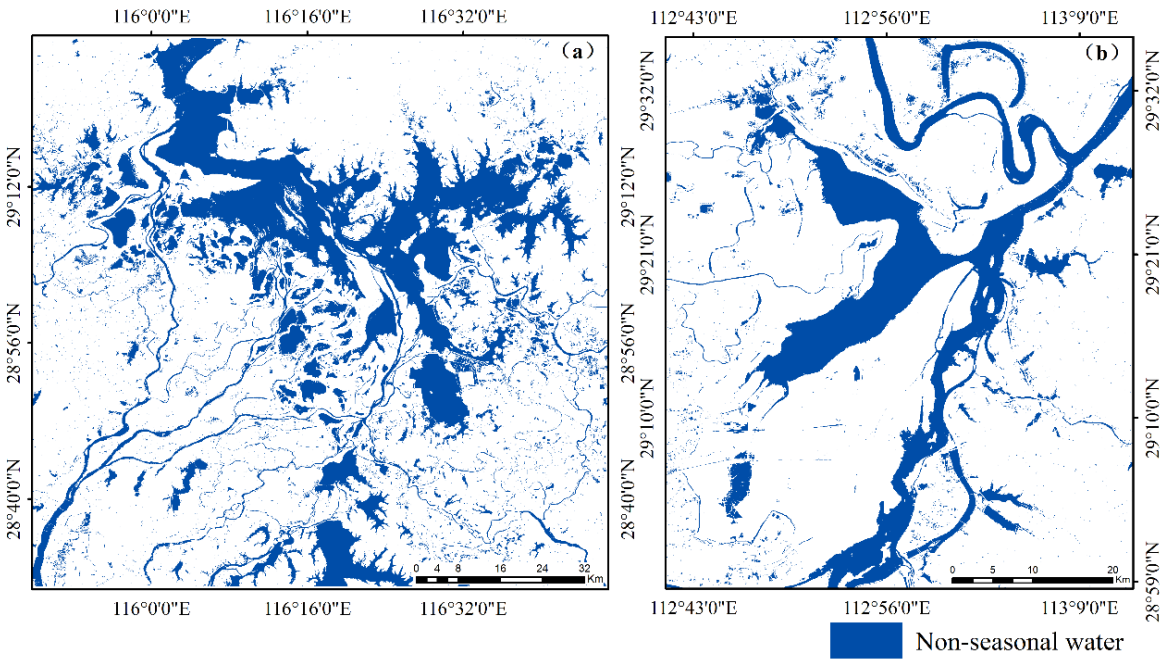


Figure 7. Result of non-seasonal water bodies. (**a**) The non-seasonal water bodies of Poyang Lake, (**b**) The non-seasonal water bodies of East Dongting Lake.

Through the comparative analysis in Figure 9, it is evident that all four methods perform well in classifying the overall flood inundation areas; however, discrepancies exist in the local flood classification results, as shown in the red-boxed areas in the Figure 10. As shown in Figure 10a,b, the method proposed in this study provides clearer classification

details along the lake edges, while the NDFI, RI, and DII methods exhibit noticeable speckling in the edge regions. Figure 10c,d demonstrate that, in the classification of small rivers, the use of NDFI, RI, and DII methods leads to misclassification, with some non-seasonal water bodies erroneously identified as flood areas.

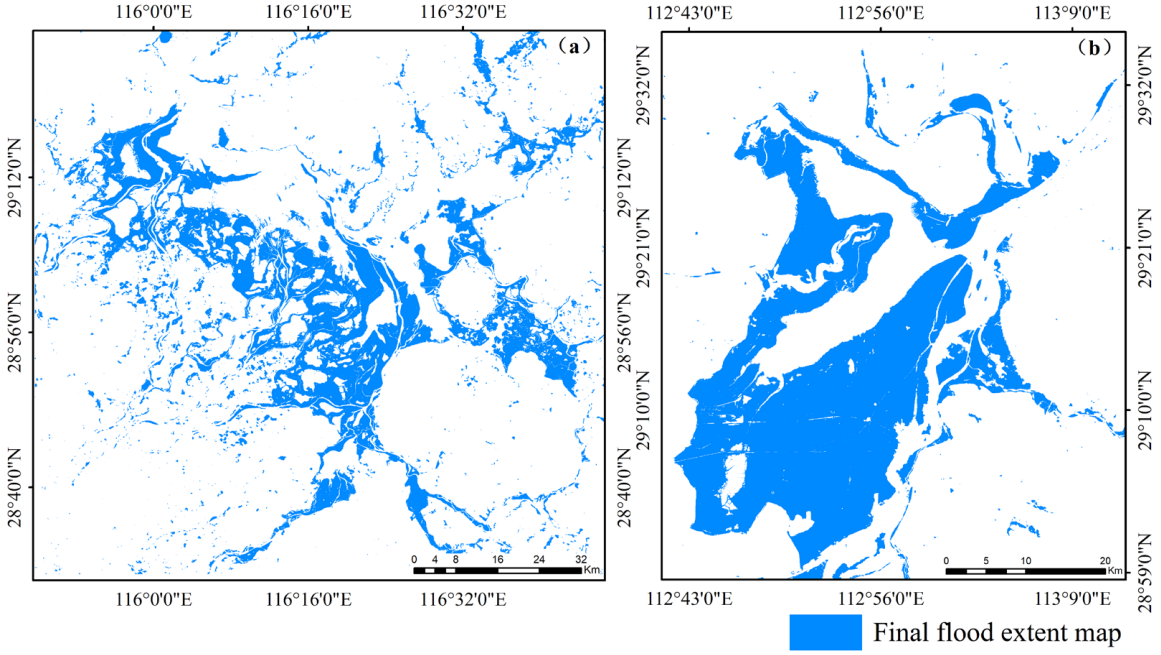


Figure 8. Result of the final flood classification. (**a**) Poyang Lake, (**b**) East Dongting Lake.

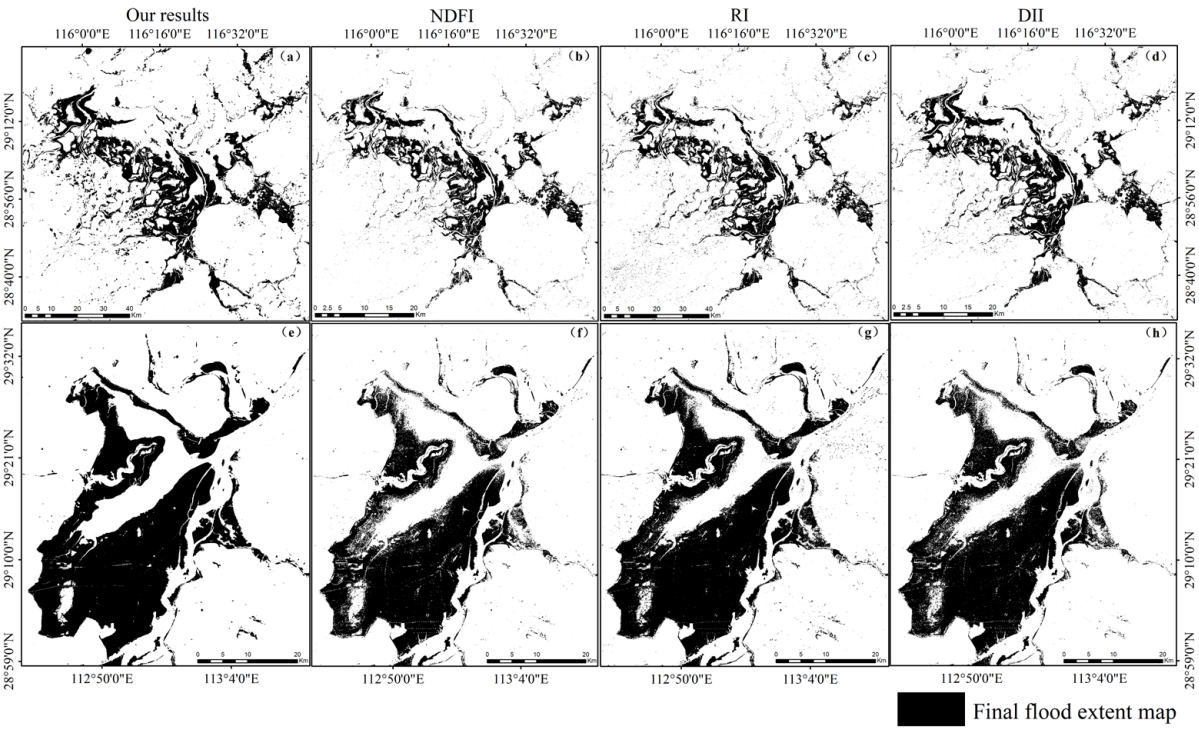


Figure 9. Contrasting the proposed method with three different methods. (**a**) Flooded area of Poyang Lake using the proposed method, (**b**) Flooded area of Poyang Lake using NDFI, (**c**) Flooded area of Poyang Lake using RI, (**d**) Flooded area of Poyang Lake using DII, (**e**) Flooded area of East Dongting Lake using the proposed method, (**f**) Flooded area of East Dongting Lake using NDFI, (**g**) Flooded area of East Dongting Lake using RI, (**h**) Flooded area of East Dongting Lake using DII.

To quantitatively assess the efficacy of the proposed method in classifying flood areas, a buffer zone was created within the study area, encompassing flood classification results for both regions. The "Create Random Points" tool in ArcGIS 10.8 was used to generate 500 random points within each buffer zone, aiming to adequately represent the characteristics of the entire dataset. Figure 11 displays the distribution of validation points. These points were visually interpreted using the Global Surface Water dataset and Sentinel-2 imagery from before and after the flood and were categorized into flooded and non-flooded areas. The criteria for classification were mainly founded on the features of water bodies and the seasonal water data present in the dataset. Since the Global Surface Water dataset is updated only until 2020, for the 2024 Poyang Lake flood, Sentinel-2 and Sentinel-1 imagery from before and after the flood were used for visual interpretation of the sample point attributes.

The classification validation points were compared with the flood area classification results using four validation metrics: precision, accuracy, F1-score, and Kappa coefficient, with the results shown in Table 2. The proposed method shows excellent validation performance in the two study areas, as indicated by the results, with all metrics surpassing those of the other three methods. Among the other indices, DII yields relatively higher metrics in the Poyang Lake region, while RI achieves relatively higher metrics in the East Dongting Lake region. In the classification of Poyang Lake, the accuracy of the proposed method is 2.2% higher than NDFI, 2.6% higher than RI, and 1.8% higher than DII. In the classification of East Dongting Lake, the proposed method's accuracy is 1.8% higher than NDFI, 1.0% higher than RI, and 2.2% higher than DII. This demonstrates the effectiveness of the flood classification results, attaining a commendable level of accuracy.

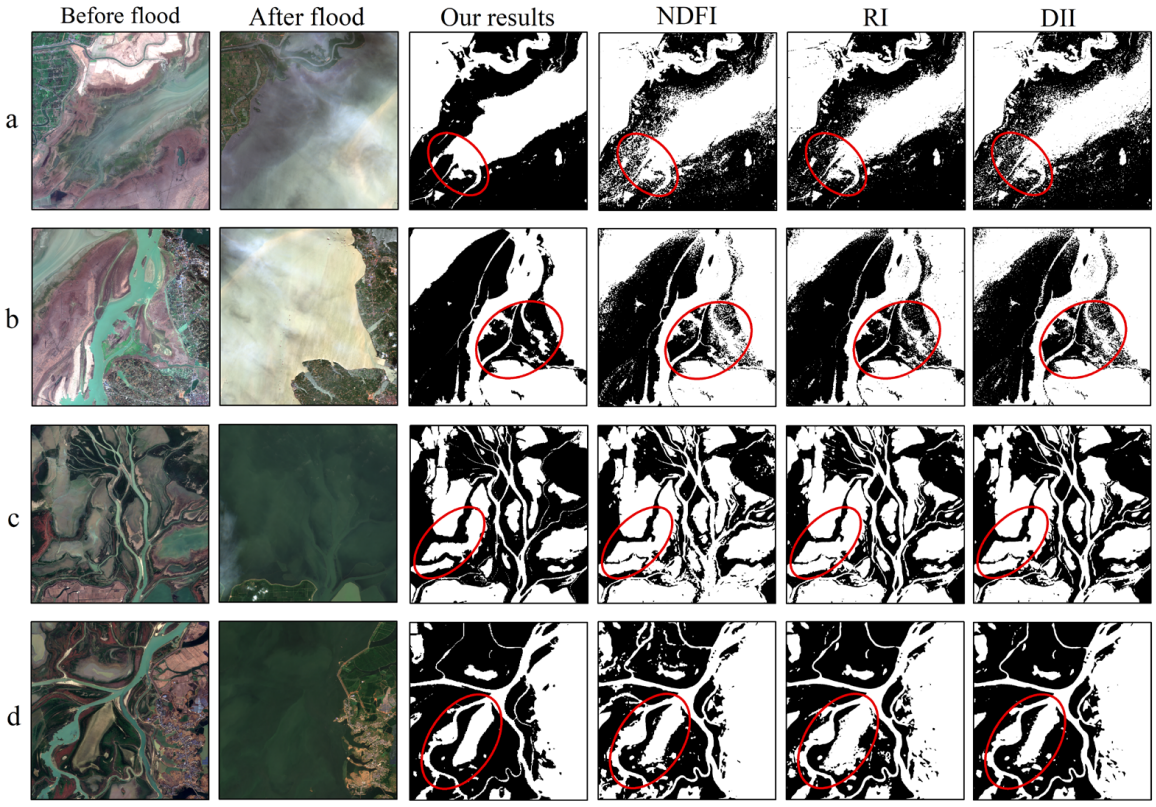


Figure 10. Detailed comparison of the proposed method with three other methods. (**a**,**b**) Local area of East Dongting Lake, (**c**,**d**) Local area of Poyang Lake.

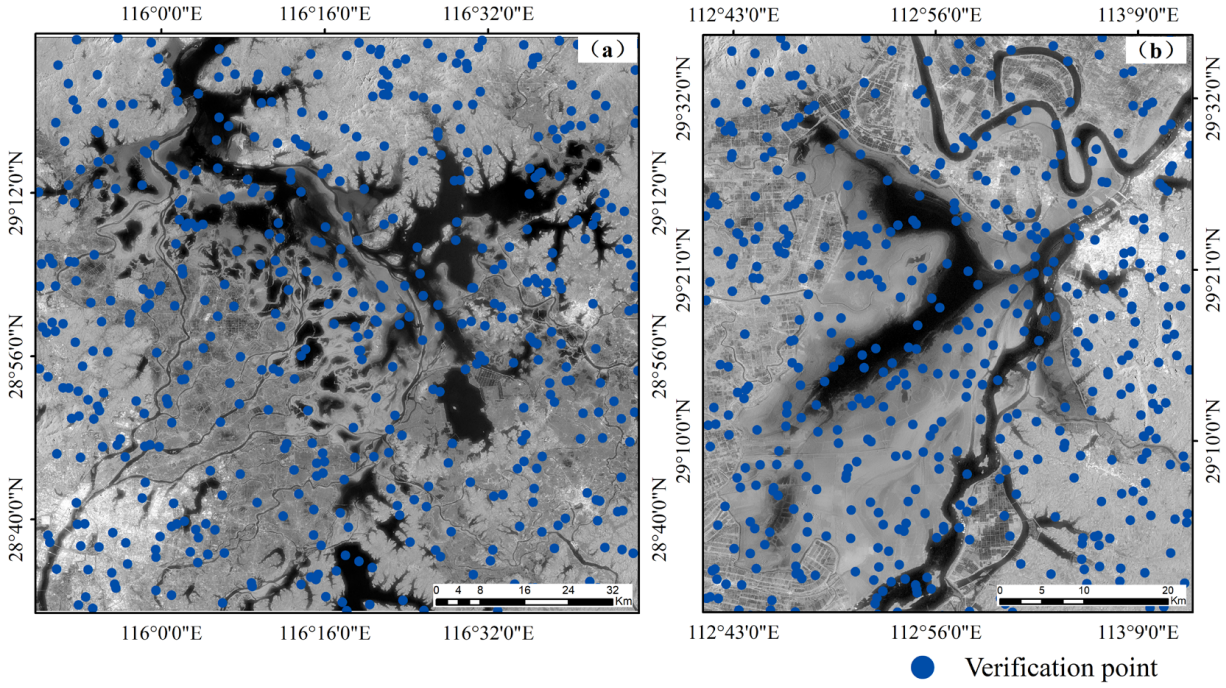


Figure 11. The distribution map of validation points in the study area. (**a**) The Poyang Lake, (**b**) The East Dongting Lake.

Table 2. Flood extraction accuracy assessment results.

Lake	Method	Precision (%)	F1-Score (%)	Accuracy (%)	Kappa (%)
Poyang Lake	NDFI	91.30	94.33	90.40	63.38
	RI	91.84	94.03	90.00	63.28
	DII	92.51	94.50	90.80	66.53
	Our results	96.50	95.43	92.60	76.07
East Dongting Lake	NDFI	95.53	96.75	95.40	88.90
	RI	97.69	97.27	96.20	91.04
	DII	95.51	96.45	95.00	87.98
	Our results	98.27	97.99	97.20	93.38

4. Discussion

4.1. Flood Inundation Map Accuracy

The production of rapid and near-real-time flood inundation maps is essential for assessing post-disaster situations and facilitating relief efforts. Existing flood extraction methods remain suboptimal and require further refinement. To efficiently and accurately obtain flood information, this study introduces an enhanced automated flood monitoring process utilizing Sentinel-1 and Landsat-8 imagery. Initially, the NDFVI index is innovatively combined with the Edge Otsu method for the initial classification of flood inundation areas, leveraging the strengths of both approaches in analyzing Sentinel-1 imagery. Subsequently, leveraging Landsat-8 imagery, non-seasonal water bodies were classified as exclusion layers through the integration of multi-index approaches and probability distribution techniques. Finally, pixels misclassified as flooded areas, which correspond to non-seasonal water bodies, are removed, yielding the final flood inundation classification map.

Research has indicated that the use of SAR imagery for change detection during floods, when combined with pre-flood optical images, effectively enhances classification accuracy [36]. Although change detection methods provide clear images of flooded areas, threshold selection must be adjusted according to the specific affected region, presenting

certain limitations. Therefore, adaptive threshold methods are adopted in this study to achieve more effective rapid flood monitoring. Some studies have compared the Otsu threshold method with machine learning approaches, demonstrating the capability of automatic Otsu thresholding for water body detection using Sentinel-1 SAR data [38]. However, there remains room for improvement in classification results [39]. The Edge Otsu method is applied to flood classification in this paper, demonstrating superior performance. Compared to threshold classification methods that utilize NDFI, DII, and RI [27], the method proposed in this study, when applied to the Poyang Lake and East Dongting Lake areas, demonstrates superior performance in flood classification. The results indicate an approximately 2% increase in accuracy, a 1% improvement in F1-score, and at least a 2% enhancement in precision and Kappa coefficients when compared to the other three methods. The method proposed in this study combines the advantages of Sentinel-1 imagery, NDFVI, and Edge Otsu in flood edge detection, while also utilizing non-seasonal water bodies classified from pre-flood Landsat-8 imagery to mask the Sentinel-1 classification results, effectively reducing errors caused by overclassification.

4.2. Limitations and Future Prospects

The annual spatial and temporal variations in the availability of remote sensing images significantly impact research outcomes, as variations in image quantity and quality can impact classification results. For instance, while Sentinel-1 SAR data are accessible within hours of a satellite pass, its temporal resolution varies across regions. Such variability may hinder the timely observation of flood dynamics. Annual fluctuations in the availability of optical images also affect assessments of non-seasonal water bodies. Therefore, improved technological capabilities and data support are crucial for attaining higher temporal resolution in effective flood emergency management. The use of multiple images and real-time data can help reduce uncertainty in flood extent validation. In the future, the development of more refined multi-source data fusion algorithms will be critical for improving flood extraction accuracy. Additionally, the employment of commercial satellites and drones to improve temporal resolution for more accurate capture of flood dynamics is suggested. It is anticipated that subsequent research will yield significant breakthroughs in the field of remote sensing data extraction for flood information.

5. Conclusions

An innovative automated method is presented in this study for the rapid classification of flood extents using multi-source and multi-temporal imagery, leveraging the capabilities of the GEE. This study combines the NDFVI and Edge Otsu methods, utilizing Sentinel-1 imagery for the preliminary extraction of flood areas. Additionally, Landsat-8 imagery is utilized to delineate non-seasonal water bodies, thereby improving the accuracy of flood-affected area identification. The excellent classification performance achieved through the combination of NDFVI and Edge Otsu is ensured by this method. Additionally, non-seasonal water bodies are effectively utilized as an exclusion layer, thereby reducing classification errors. This method was applied to the 2020 Poyang Lake and 2024 East Dongting Lake floods as case studies. Compared with NDFI, RI, and DII flood classification methods, accuracy improvements of 2% or more for the Poyang Lake flood event and 1% or more for the East Dongting Lake flood event were achieved, outperforming other methods. This new method provides an effective solution for flood area classification, characterized by low cost, high accuracy, high efficiency, and ease of implementation, rendering it suitable for flood disaster monitoring under extreme weather conditions. Timely and accurate technical support is offered to decision-makers and emergency response teams.

Author Contributions: Methodology, X.P. and Z.M.; validation, X.P. and Y.X.; writing—original draft preparation, X.P.; writing—review and editing, X.P., S.C., Z.M., Y.X., M.Y. and P.L.; funding acquisition, S.C. All authors have read and agreed to the published version of the manuscript.

Funding: Changchun Satellite and Application Industry Major Science and Technology Project (grant No. 2024WX06).

Data Availability Statement: The original contributions presented in this study are included in the article. Further inquiries can be directed to the corresponding author.

Conflicts of Interest: The authors declare no conflicts of interest.

References

1. Zheng, G.; Allen, S.K.; Bao, A.; Ballesteros-Cánovas, J.A.; Huss, M.; Zhang, G.; Li, J.; Yuan, Y.; Jiang, L.; Yu, T. Increasing risk of glacial lake outburst floods from future third pole deglaciation. *Nat. Clim. Chang.* **2021**, *11*, 411–417. [CrossRef]
2. Grimaldi, S.; Xu, J.; Li, Y.; Pauwels, V.R.; Walker, J.P. Flood Mapping under Vegetation Using Single SAR Acquisitions. *Remote Sens. Environ.* **2020**, *237*, 111582. [CrossRef]
3. Munawar, H.S.; Hammad, A.W.; Waller, S.T. A review on flood management technologies related to image processing and machine learning. *Autom. Constr.* **2021**, *132*, 103916. [CrossRef]
4. Liang, J.; Liu, D. A local thresholding approach to flood water delineation using Sentinel-1 SAR imagery. *ISPRS J. Photogramm. Remote Sens.* **2020**, *159*, 53–62. [CrossRef]
5. Jafarzadegan, K.; Muñoz, D.F.; Moftakhari, H.; Gutenson, J.L.; Savant, G.; Moradkhani, H. Real-time coastal flood hazard assessment using DEM-based hydrogeomorphic classifiers. *Nat. Hazards Earth Syst. Sci.* **2022**, *22*, 1419–1435. [CrossRef]
6. Ulloa, N.I.; Yun, S.-H.; Chiang, S.-H.; Furuta, R. Sentinel-1 spatiotemporal simulation using convolutional LSTM for flood mapping. *Remote Sens.* **2022**, *14*, 246. [CrossRef]
7. Li, J.; Wang, C.; Xu, L.; Wu, F.; Zhang, H.; Zhang, B. Multitemporal water extraction of dongting lake and poyang lake based on an automatic water extraction and dynamic monitoring framework. *Remote Sens.* **2021**, *13*, 865. [CrossRef]
8. DeVries, B.; Huang, C.; Armston, J.; Huang, W.; Jones, J.W.; Lang, M.W. Rapid and robust monitoring of flood events using Sentinel-1 and Landsat data on the Google Earth Engine. *Remote Sens. Environ.* **2020**, *240*, 111664. [CrossRef]
9. McFeeters, S.K. The use of the Normalized Difference Water Index (NDWI) in the delineation of open water features. *Int. J. Remote Sens.* **1996**, *17*, 1425–1432. [CrossRef]
10. Xu, H. Modification of normalised difference water index (NDWI) to enhance open water features in remotely sensed imagery. *Int. J. Remote Sens.* **2006**, *27*, 3025–3033. [CrossRef]
11. Yan, P.; Zhang, Y.; Zhang, Y. A study on information extraction of water system in semi-arid regions with the enhanced water index (EWI) and GIS based noise remove techniques. *Remote Sens. Inf.* **2007**, *6*, 62–67.
12. Tulbure, M.G.; Broich, M.; Stehman, S.V.; Kommareddy, A. Surface water extent dynamics from three decades of seasonally continuous Landsat time series at subcontinental scale in a semi-arid region. *Remote Sens. Environ.* **2016**, *178*, 142–157. [CrossRef]
13. Feyisa, G.L.; Meilby, H.; Fensholt, R.; Proud, S.R. Automated Water Extraction Index: A new technique for surface water mapping using Landsat imagery. *Remote Sens. Environ.* **2014**, *140*, 23–35. [CrossRef]
14. Zou, Z.; Xiao, X.; Dong, J.; Qin, Y.; Doughty, R.B.; Menarguez, M.A.; Zhang, G.; Wang, J. Divergent trends of open-surface water body area in the contiguous United States from 1984 to 2016. *Proc. Natl. Acad. Sci. USA* **2018**, *115*, 3810–3815. [CrossRef]
15. Han, Y.; Deng, F.; Gong, J.; Li, Z.; Liu, Z.; Zhang, J.; Liu, W. Water distribution based on SAR and optical data to improve hazard mapping. *Environ. Res.* **2023**, *235*, 116694. [CrossRef]
16. Singha, M.; Dong, J.; Sarmah, S.; You, N.; Zhou, Y.; Zhang, G.; Doughty, R.; Xiao, X. Identifying floods and flood-affected paddy rice fields in Bangladesh based on Sentinel-1 imagery and Google Earth Engine. *ISPRS J. Photogramm. Remote Sens.* **2020**, *166*, 278–293. [CrossRef]
17. Bauer-Marschallinger, B.; Cao, S.; Tupas, M.E.; Roth, F.; Navacchi, C.; Melzer, T.; Freeman, V.; Wagner, W. Satellite-Based Flood Mapping through Bayesian Inference from a Sentinel-1 SAR Datacube. *Remote Sens.* **2022**, *14*, 3673. [CrossRef]
18. Shen, X.; Anagnostou, E.N.; Allen, G.H.; Brakenridge, G.R.; Kettner, A.J. Near-real-time non-obstructed flood inundation mapping using synthetic aperture radar. *Remote Sens. Environ.* **2019**, *221*, 302–315. [CrossRef]
19. Dasgupta, A.; Grimaldi, S.; Ramsankaran, R.; Pauwels, V.R.; Walker, J.P.; Chini, M.; Hostache, R.; Matgen, P. Flood mapping using synthetic aperture radar sensors from local to global scales. In *Global Flood Hazard: Applications in Modeling, Mapping, and Forecasting*; Wiley: Hoboken, NJ, USA, 2018; pp. 55–77.
20. Benoudjit, A.; Guida, R. A novel fully automated mapping of the flood extent on SAR images using a supervised classifier. *Remote Sens.* **2019**, *11*, 779. [CrossRef]

21. Parsian, S.; Amani, M.; Moghimi, A.; Ghorbanian, A.; Mahdavi, S. Flood hazard mapping using fuzzy logic, analytical hierarchy process, and multi-source geospatial datasets. *Remote Sens.* **2021**, *13*, 4761. [CrossRef]
22. Hashemi-Beni, L.; Gebrehiwot, A.A. Flood extent mapping: An integrated method using deep learning and region growing using UAV optical data. *IEEE J. Sel. Top. Appl. Earth Obs. Remote Sens.* **2021**, *14*, 2127–2135. [CrossRef]
23. Clement, M.A.; Kilsby, C.G.; Moore, P. Multi-temporal synthetic aperture radar flood mapping using change detection. *J. Flood Risk Manag.* **2018**, *11*, 152–168. [CrossRef]
24. Amitrano, D.; Di Martino, G.; Iodice, A.; Riccio, D.; Ruello, G. Unsupervised rapid flood mapping using Sentinel-1 GRD SAR images. *IEEE Trans. Geosci. Remote Sens.* **2018**, *56*, 3290–3299. [CrossRef]
25. Schlaffer, S.; Chini, M.; Giustarini, L.; Matgen, P. Probabilistic mapping of flood-induced backscatter changes in SAR time series. *Int. J. Appl. Earth Obs. Geoinf.* **2017**, *56*, 77–87. [CrossRef]
26. Bovolo, F.; Bruzzone, L. A detail-preserving scale-driven approach to change detection in multitemporal SAR images. *IEEE Trans. Geosci. Remote Sens.* **2005**, *43*, 2963–2972. [CrossRef]
27. Cian, F.; Marconcini, M.; Ceccato, P. Normalized Difference Flood Index for rapid flood mapping: Taking advantage of EO big data. *Remote Sens. Environ.* **2018**, *209*, 712–730. [CrossRef]
28. Vanama, V.; Rao, Y.; Bhatt, C. Change detection based flood mapping using multi-temporal Earth Observation satellite images: 2018 flood event of Kerala, India. *Eur. J. Remote Sens.* **2021**, *54*, 42–58. [CrossRef]
29. Qiu, J.; Cao, B.; Park, E.; Yang, X.; Zhang, W.; Tarolli, P. Flood monitoring in rural areas of the Pearl River Basin (China) using Sentinel-1 SAR. *Remote Sens.* **2021**, *13*, 1384. [CrossRef]
30. Jia, M.; Zhao, Z.; Huo, L.; Chen, H.; Qiu, Y. Incorporating global-local a Priori knowledge into expectation-maximization for SAR image change detection. *Int. J. Remote Sens.* **2019**, *40*, 734–758. [CrossRef]
31. Borghys, D.; Yvinec, Y.; Perneel, C.; Pizurica, A.; Philips, W. Supervised feature-based classification of multi-channel SAR images. *Pattern Recognit. Lett.* **2006**, *27*, 252–258. [CrossRef]
32. Sun, Y.; Lei, L.; Li, X.; Tan, X.; Kuang, G. Structure consistency-based graph for unsupervised change detection with homogeneous and heterogeneous remote sensing images. *IEEE Trans. Geosci. Remote Sens.* **2021**, *60*, 1–21. [CrossRef]
33. Brisco, B.; Short, N.; Sanden, J.v.d.; Landry, R.; Raymond, D. A semi-automated tool for surface water mapping with RADARSAT-1. *Can. J. Remote Sens.* **2009**, *35*, 336–344. [CrossRef]
34. Tsyganskaya, V.; Martinis, S.; Marzahn, P.; Ludwig, R. Detection of temporary flooded vegetation using Sentinel-1 time series data. *Remote Sens.* **2018**, *10*, 1286. [CrossRef]
35. Tarpanelli, A.; Mondini, A.C.; Camici, S. Effectiveness of Sentinel-1 and Sentinel-2 for flood detection assessment in Europe. *Nat. Hazards Earth Syst. Sci.* **2022**, *22*, 2473–2489. [CrossRef]
36. Xue, F.; Gao, W.; Yin, C.; Chen, X.; Xia, Z.; Lv, Y.; Zhou, Y.; Wang, M. Flood monitoring by integrating normalized difference flood index and probability distribution of water bodies. *IEEE J. Sel. Top. Appl. Earth Obs. Remote Sens.* **2022**, *15*, 4170–4179. [CrossRef]
37. Chini, M.; Hostache, R.; Giustarini, L.; Matgen, P. A hierarchical split-based approach for parametric thresholding of SAR images: Flood inundation as a test case. *IEEE Trans. Geosci. Remote Sens.* **2017**, *55*, 6975–6988. [CrossRef]
38. Bangira, T.; Alfieri, S.M.; Menenti, M.; Van Niekerk, A. Comparing thresholding with machine learning classifiers for mapping complex water. *Remote Sens.* **2019**, *11*, 1351. [CrossRef]
39. Wang, Z.; Xie, F.; Ling, F.; Du, Y. Monitoring surface water inundation of Poyang Lake and Dongting Lake in China using Sentinel-1 SAR images. *Remote Sens.* **2022**, *14*, 3473. [CrossRef]
40. Markert, K.N.; Markert, A.M.; Mayer, T.; Nauman, C.; Haag, A.; Poortinga, A.; Bhandari, B.; Thwal, N.S.; Kunlamai, T.; Chishtie, F. Comparing sentinel-1 surface water mapping algorithms and radiometric terrain correction processing in southeast asia utilizing google earth engine. *Remote Sens.* **2020**, *12*, 2469. [CrossRef]
41. Wu, H.; Chen, J.; Zeng, G.; Xu, J.; Sang, L.; Liu, Q.; Dai, J.; Xiong, W.; Yuan, Z.; Wang, Y. Effects of Early Dry Season on Habitat Suitability for Migratory Birds in China's Two Largest Freshwater Lake Wetlands after the Impoundment of Three Gorges Dam. *J. Environ. Inform.* **2020**, *36*, 82–92. [CrossRef]
42. Wu, G.; Liu, Y. Mapping dynamics of inundation patterns of two largest river-connected lakes in China: A comparative study. *Remote Sens.* **2016**, *8*, 560. [CrossRef]
43. Notti, D.; Giordan, D.; Caló, F.; Pepe, A.; Zucca, F.; Galve, J.P. Potential and limitations of open satellite data for flood mapping. *Remote Sens.* **2018**, *10*, 1673. [CrossRef]
44. Dao, P.D.; Liou, Y.-A. Object-based flood mapping and affected rice field estimation with Landsat 8 OLI and MODIS data. *Remote Sens.* **2015**, *7*, 5077–5097. [CrossRef]
45. Malenovský, Z.; Rott, H.; Cihlar, J.; Schaepman, M.E.; García-Santos, G.; Fernandes, R.; Berger, M. Sentinels for science: Potential of Sentinel-1,-2, and-3 missions for scientific observations of ocean, cryosphere, and land. *Remote Sens. Environ.* **2012**, *120*, 91–101. [CrossRef]
46. Schlaffer, S.; Chini, M.; Dorigo, W.; Plank, S. Monitoring surface water dynamics in the Prairie Pothole Region of North Dakota using dual-polarised Sentinel-1 synthetic aperture radar (SAR) time series. *Hydrol. Earth Syst. Sci.* **2022**, *26*, 841–860. [CrossRef]

47. Song, L.; Song, C.; Luo, S.; Chen, T.; Liu, K.; Li, Y.; Jing, H.; Xu, J. Refining and densifying the water inundation area and storage estimates of Poyang Lake by integrating Sentinel-1/2 and bathymetry data. *Int. J. Appl. Earth Obs. Geoinf.* **2021**, *105*, 102601. [CrossRef]
48. Pekel, J.-F.; Cottam, A.; Gorelick, N.; Belward, A.S. High-resolution mapping of global surface water and its long-term changes. *Nature* **2016**, *540*, 418–422. [CrossRef] [PubMed]
49. Hoekman, D.H.; Reiche, J. Multi-model radiometric slope correction of SAR images of complex terrain using a two-stage semi-empirical approach. *Remote Sens. Environ.* **2015**, *156*, 1–10. [CrossRef]
50. Abo Gharbia, A.Y.; Amin, M.; Mousa, A.E.; AbouAly, N.; El Banby, G.M.; Abd El-Samie, F.E. Registration-based change detection for SAR images. *NRIAG J. Astron. Geophys.* **2020**, *9*, 106–115. [CrossRef]
51. Donchyts, G.; Schellekens, J.; Winsemius, H.; Eisemann, E.; Van de Giesen, N. A 30 m resolution surface water mask including estimation of positional and thematic differences using landsat 8, srtm and openstreetmap: A case study in the Murray-Darling Basin, Australia. *Remote Sens.* **2016**, *8*, 386. [CrossRef]
52. Deng, Y.; Jiang, W.; Tang, Z.; Ling, Z.; Wu, Z. Long-term changes of open-surface water bodies in the Yangtze River basin based on the Google Earth Engine cloud platform. *Remote Sens.* **2019**, *11*, 2213. [CrossRef]
53. Zhou, H.; Liu, S.; Hu, S.; Mo, X. Retrieving dynamics of the surface water extent in the upper reach of Yellow River. *Sci. Total Environ.* **2021**, *800*, 149348. [CrossRef]
54. Li, Z.; Zhang, X.; Xiao, P. Spectral index-driven FCN model training for water extraction from multispectral imagery. *ISPRS J. Photogramm. Remote Sens.* **2022**, *192*, 344–360. [CrossRef]
55. Huete, A.; Didan, K.; Miura, T.; Rodriguez, E.P.; Gao, X.; Ferreira, L.G. Overview of the radiometric and biophysical performance of the MODIS vegetation indices. *Remote Sens. Environ.* **2002**, *83*, 195–213. [CrossRef]
56. Liu, X.; Hu, G.; Chen, Y.; Li, X.; Xu, X.; Li, S.; Pei, F.; Wang, S. High-resolution multi-temporal mapping of global urban land using Landsat images based on the Google Earth Engine Platform. *Remote Sens. Environ.* **2018**, *209*, 227–239. [CrossRef]

Disclaimer/Publisher's Note: The statements, opinions and data contained in all publications are solely those of the individual author(s) and contributor(s) and not of MDPI and/or the editor(s). MDPI and/or the editor(s) disclaim responsibility for any injury to people or property resulting from any ideas, methods, instructions or products referred to in the content.